Article

pubs.acs.org/Biomac

Bioactive Cellulose Nanofibrils for Specific Human IgG Binding

Yanxia Zhang,*[,†] Ruben G. Carbonell,[‡] and Orlando J. Rojas*[,†,‡,§]

Departments of [†]Forest Biomaterials and [‡]Chemical and Biomolecular Engineering, North Carolina State University, Raleigh, North Carolina 27695, United States

[§]School of Science and Technology, Department of Forest Products Technology, Aalto University, 00076 Aalto, Finland

Supporting Information

ABSTRACT: Bioactive films were produced by conjugation of a short peptide onto modified cellulose nanofibrils (CNF). Specifically, a hydrophilic copolymer, poly(2-aminoethyl methacrylate hydrochloride-*co*-2-hydroxyethyl-methacrylate) (poly(AMA-*co*-HEMA)), was grafted via surface initiated polymerization from an initiator coupled to CNF. The poly(AMA-*co*-HEMA) was used as a spacer and support layer for immobilization of the peptide, acetylated-HWRGWVA, which has specific affinity with human immunoglobulin G (hIgG). Two methods for peptide grafting were compared: modification of CNF in aqueous suspension followed by assembly into a bioactive film and peptide grafting on a preformed CNF film. The CNF-based networks were examined on solid supports via atomic force microscopy (AFM) and extreme resolution imaging with ultralow electron landing energies (scanning low energy electron microscopy). The specific binding capability of hIgG and nonspecific protein resistance of the resultant peptide-modified CNF were evaluated by using quartz crystal microgravimetry (QCM). The effects of initiator concentration and thickness of poly(AMA-*co*-HEMA) layer on hIgG adsorption were investigated in the developed systems, which exhibited high signal-to-noise response.

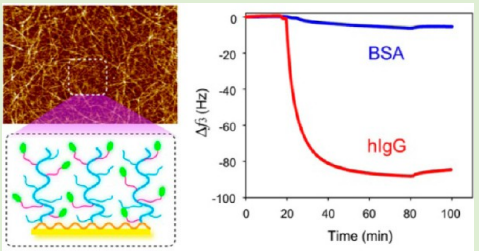

INTRODUCTION

Cellulose nanofibrils (CNF), also known as nanofibrillar cellulose (NFC), enables the formation of very strong and dense network structures, such as nanopaper, owing to the high aspect ratio of the constituent units, fibrils with lengths in the micrometer and widths in the nanometer scales. CNF is typically produced from wood fibers via mechanical disintegration with optional chemical or enzymatic pretreatments.[1−4] Besides the inherent advantages of cellulose, such as good biocompatibility, nontoxicity, and biodegradability,[5,6] CNF is insoluble in most solvents, has a high surface area, and excellent mechanical strength due to its unique nanostructure.[7,8] In addition, CNF surfaces have abundant free hydroxyl groups, which not only hold a large capability for water adsorption and to create a hydrophilic microenvironment, but they also can be easily activated by different coupling agents.[9−12] The above features give CNF a great potential as a novel platform in the biomedical and bioengineering fields.[13] In the past decades, a considerable number of authors have reported on the use of CNF in pharmaceutics,[14,15] cell culture and tissue engineering,[16] antimicrobial agents,[17] and biosensors and diagnostics.[11,12] CNF has both amorphous and crystalline cellulose I regions,[18,19] as presented in native cellulose, and it can be used in ultrathin films or nanopaper as a model system to monitor molecular interactions using surface-sensitive methods such as quartz crystal microgravimetry (QCM),[11,12] surface plasmon resonance (SPR),[20] and atomic force microscopy (AFM).[18,21] In addition, CNF provides an ideal platform for development of paper-based diagnostic and analytical devices.

Previous research suggested that CNF is a good candidate for immobilization of functional biomolecules, which is of crucial importance in various applications.[11−13] However, due to the inherent bioinertness of CNF, proper activation or modification is necessary before conjugation of biomolecules. For example, Arola et al. used several coupling agents to convert the hydroxyl groups of CNF to functional groups (amine, epoxy, and carboxylic acid) and conjugated a model protein, alkaline phosphatase, onto its surface through covalent chemistries.[13] Orelma et al. carboxylated CNF via (2,2,6,6-tetramethylpiperidin-1-yl)oxyl (TEMPO) oxidation and then immobilized avidin[12] and antihuman immunoglobulin G (anti-hIgG)[11] to detect biotinylated anti-hIgG or hIgG. However, a drawback in these reported methods is the potential loss of bioactivity resulting from the biomolecules bound directly to the CNF surfaces. Moreover, the chemical modification of hydroxyl groups might reduce the resistance to nonspecific interactions, leading to unwanted interference or bioresponse. An effective way to overcome these issues is the use of (co)polymer spacers for immobilization of biomolecules and thus achieves "bioactive" surfaces.[6] Although this strategy has been widely adopted for different types of substrates and materials, to our knowledge it has not been applied to CNF substrates.

hIgG is the second most abundant protein in human blood (concentration of 6.6 to 14.5 mg/mL in normal human plasma) and is a major component of the immune system.[22,23] Many

Received: June 4, 2013
Revised: July 29, 2013

   dx.doi.org/10.1021/bm4007979 | *Biomacromolecules* XXXX, XXX, XXX−XXX

Scheme 1. (Left) Schematic Illustration of the Preparation of Peptide-CNF Films for hIgG Detection by Using Two Different Methods (Methods I and II); (Right) Generic Chemical Reactions in Step ② of the Modifications; (bottom panel) Bioconjuation of Peptide on Copolymer with HATU Chemistry Involved in Step ③ of the Modifications

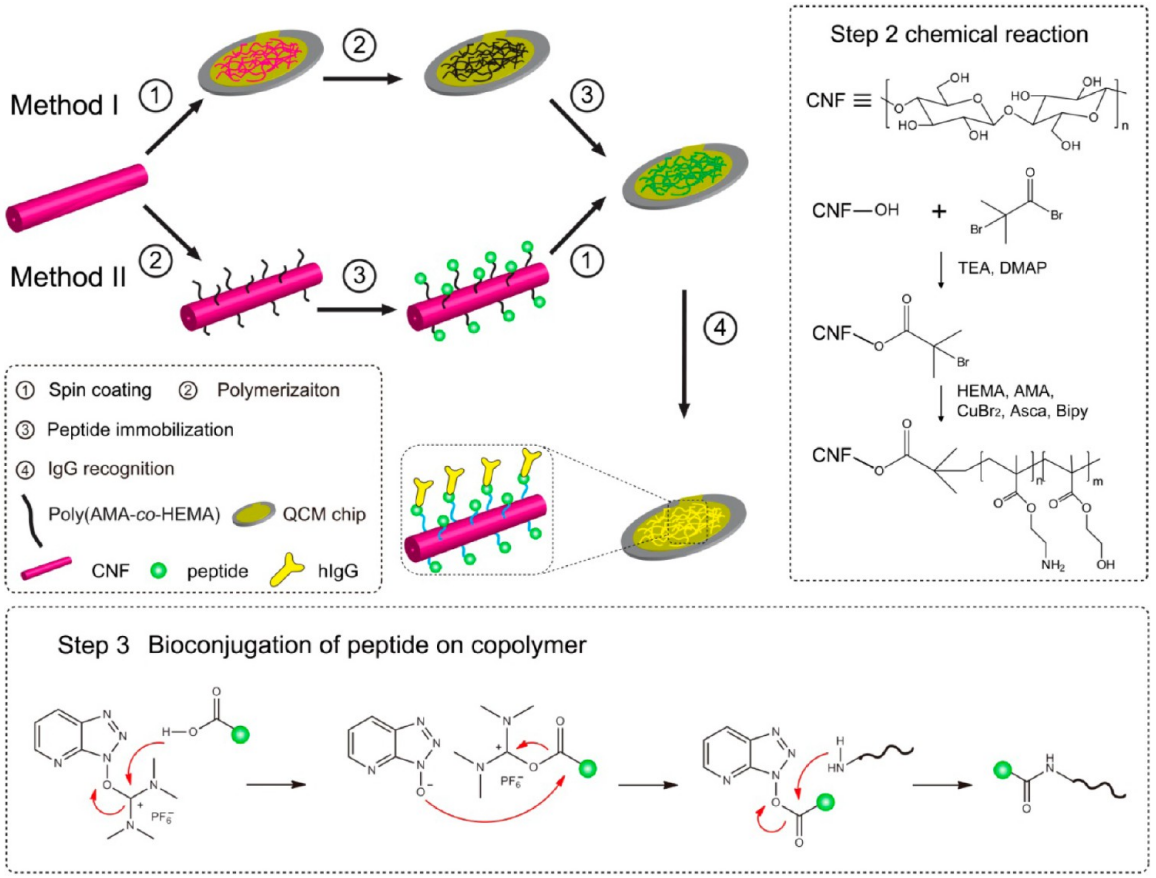

autoimmune diseases are related to hIgG and its concentration levels are generally indicative of an individual's immune status to particular pathogens.[24−26] Therefore, techniques for detecting hIgG are of great interest. We previously developed a peptide-based sensor using poly(2-aminoethyl methacrylate hydrochloride-*co*-2-hydroxyethyl methacrylate) (poly(AMA-*co*-HEMA)) as spacer. The two components AMA and HEMA provided peptide-binding sites and nonspecific resistance, respectively. The resultant surface exhibited high signal-to-noise response and excellent detection limits for target hIgG.[27,28]

In this work, we exploit the potential of CNF as substrate for immobilization of biomolecules using the same copolymers as anchoring spacers. Atom transfer radical polymerization (ATRP) initiators were first attached onto CNF surfaces,[29,30] and poly(AMA-*co*-HEMA) was then grafted from the initiator-modified CNF. Acetylated-HWRGWVA (Ac-HWRGWVA) peptide, which has high specific affinity to hIgG[31−35] was conjugated to AMA segments via covalent amide bonds. The specific binding capability of hIgG and nonspecific protein resistance of the resultant peptide-CNF surface were evaluated using QCM. The significance of this work is 2-fold. From a fundamental point of view, the investigation of protein adsorption on functionalized CNF furthers our understanding of cellulose-biomolecule interactions. From a practical application point of view, the proposed strategy provides a facile and versatile method for development of CNF as a nanopaper for biosensing and detection or as a static chromatography phase.

MATERIALS AND METHODS

Materials. CNF suspension (solid content is 1.6%) was prepared as previously reported.[11] Briefly, bleached hardwood (birch) kraft pulp was mechanically treated (five passes in a Masuko grinder) and then further disintegrated via microfluidization (20 passes). QCM gold chips were supplied from Q-Sense (Göteborg, Sweden). Ac-HWRGWVA (95.1%) was obtained from GenScript (Piscataway, NJ). Human IgG (>97%) was purchased as a lyophilized powder from Equitech-Bio (Kerrville, TX). Poly(ethyleneimine) (PEI, 600−1000 kDa molecular weight 50% in water), 2-bromoisobutyryl bromide (BIBB), triethanolamine (TEA), 2-dimethylaminopyridine (DMAP), 2-hydroxyethyl methacrylate (HEMA), 2-aminoethyl methacrylate hydrochloride (AMA), 2,2′-bipyridine (Bipy), copper(II) bromide ($CuBr_2$), ascorbic acid (Asca, reagent grade), *O*-(7-azabenzotriazol-1-yl)-*N*,*N*,*N*′,*N*′-tetramethyluronium hexafluorophosphate (HATU), *N*,*N*-diisopropylethylamine (DIPEA), tetrahydrofuran (THF, anhydrous), *N*,*N*-dimethylformamide (DMF, anhydrous), acetone, ethanol, methanol, and albumin from bovine serum (BSA) were all purchased from Sigma-Aldrich (Milwaukee, WI) and used as received.

Surface Preparation. The short peptide was conjugated to CNF using poly(AMA-*co*-HEMA) as spacer. The peptide-functionalized CNF (peptide-CNF) was fixed as a film on QCM sensors by two different methods (see Scheme 1). In Method I the CNF suspension was spin-coated directly onto the QCM sensor followed by peptide conjugation. In Method II the peptide was immobilized to CNF in aqueous suspension, and then the peptide-CNF was spin-coated on the QCM sensor.

dx.doi.org/10.1021/bm4007979 | *Biomacromolecules* XXXX, XXX, XXX−XXX

Method I. CNF suspension was spin-coated onto QCM surface.[11] Briefly, diluted CNF suspensions (1.67 g/L in water) were homogenized with microtip-sonicator (10 min, 25% amplitude) and then centrifuged (10400 rpm, 45 min, 25 °C) to collect a clear supernatant CNF suspension. The CNF suspension was then spin-coated (Laurell Technologies Corporation WS-400-6NPP\LITE) at 3000 rpm for 1 min onto the solid support carrying a thin anchoring layer of PEI (thickness = 0.8 ± 0.2 nm). The spin-coating of CNF suspension was repeated twice in order to obtain fully covering CNF surfaces. The obtained CNF films were rinsed carefully with Milli-Q water and dry gently with nitrogen gas and stored in desiccators prior to use.

CNF surfaces were incubated in a solution of THF (20 mL), TEA (76.4 μL) and DMAP (76.4 μL) and cooled to 0 °C under argon atmosphere. Different amounts of initiator BIBB (10, 20, 40, 60 μL) were then added dropwise to the solution to adjust the initiator density on the CNF film. The reaction proceeded at 0 °C for 1 h and then left at room temperature overnight. Finally, the surfaces were rinsed with THF and Milli-Q water and dried under a nitrogen flow to achieve the initiator-CNF surfaces.

Poly(AMA-*co*-HEMA) copolymer was *grafted from* initiator-CNF via activators regenerated by electron transfer−atom transfer radical polymerization (ARGET-ATRP). The reaction solution was prepared by dissolving AMA (0.36 g, 2.2 mmol), HEMA (1.15 g, 8.8 mmol), bipyridine (7.7 mg, 49 μmol), $CuBr_2$ (1.6 mg, 7 μmol), and ascorbic acid (17.3 mg, 98 μmol) into a mixture of methanol (7 mL) and water (7 mL) and then was added to initiator-CNF surfaces at room temperature. The thickness of poly(AMA-*co*-HEMA) was controlled by changing the polymerization time from 0 to 120 min. The obtained surfaces were then thoroughly rinsed with Milli-Q water to remove any impurities and dried under nitrogen flow to obtain copolymer-CNF surfaces.

Ac-HWRGWVA peptide was immobilized onto the copolymer-CNF surface by using HATU as coupling regent in the reaction of carboxylated groups of the short peptide and the free amine groups of AMA segments.[28] Briefly, the copolymer-CNF surfaces were immersed in DMF solution (20 mL) containing Ac-HWRGWVA (5 mg/mL) and HATU (3.8 mg/mL), followed by injection of DIPEA (2.58 uL/mL) under nitrogen atmosphere for 12 h. Finally, the surfaces were thoroughly rinsed with DMF and Milli-Q water and dried with nitrogen to achieve peptide-CNF (I) surfaces.

Method II. CNF aqueous suspension (2 g) was solvent exchanged from water to acetone (50 mL, three times) and then via acetone to THF using three successive centrifugations at 12000 rpm (10 °C for 20 min) and resuspension steps for each solvent. The procedure to prepare initiator-CNF in aqueous suspension was similar to that explained in Method I, except that different amounts of THF (100 mL), TEA (2.3 mL), DMAP (2.3 mL), and BIBB (1.2 mL) were used. The product was successively washed by centrifugation with THF, THF/EtOH (1/1), acetone, and Milli-Q, respectively, to remove the free BIBB from the CNF suspensions. Copolymer-CNF was prepared in aqueous suspension following the same protocol in Method I, using 2 h as polymerization time. The resultant suspension was centrifuged and redispersed successively in Milli-Q water (12000 rpm at 25 °C for 20 min, three times), acetone (12000 rpm at 10 °C for 20 min), and DMF (12000 rpm at 10 °C for 20 min) to achieve purified copolymer-CNF. Finally, copolymer-CNF was immersed into peptide containing DMF solution as previously described. After stirring at room temperature for 12 h, the resultant suspension was centrifuged and redispersed successively in DMF, acetone, and water and then dialyzed in Milli-Q water with a 3500 MWCO dialysis membrane to remove trace amounts of residual peptides and to obtain peptide-CNF.

Peptide-CNF suspensions were spin-coated directly on UV cleaned QCM supports as was introduced earlier in Method I; different layers were applied to achieve peptide-CNF (II) surfaces. The peptide-CNF surfaces prepared by Methods I and II were stored in a refrigerator prior to use in QCM.

Surface Characterization. *Ellipsometry.* The thickness of CNF layer on the QCM sensor support was measured using a spectroscopic ellipsometer (model M-2000 V, J. A. Woollam Co., Inc.) at an angle of 70° and wavelengths from 400 to 800 nm. We assumed CNF as a polymer and used the Cauchy model for fitting the data. In Method I, we used multiple layers (CNF and copolymer layers) for fitting the data. Each of the average thickness values reported was obtained from three replicates.

Contact Angle Goniometry. Changes in the surface wettability were monitored by the static water contact angles (WCA), which were measured using a contact angle goniometer (SEO Phoenix 300, Korea) at room temperature. Each average contact angle value reported was obtained from six replicates.

Fourier Transform Infrared Spectroscopy. The changes in chemistry after the modification steps involved in Methods I and II were determined via attenuated total reflection Fourier transform infrared (ATR-FTIR) and FTIR in absorbance mode, respectively. The measurement was performed in a thermo Nicolet 670 FTIR ESP spectrometer equipped with a Smart OMNI sampler (Nicolet Instrument Corp.). For samples in Method II, the unmodified and modified CNF were freeze-dried and made into pellets with KBr. The data were collected over 128 continuous scans with a resolution of 4 cm^{-1}.

Atomic Force Microscopy. Tapping-mode topographical measurements of CNF surfaces and peptide-CNF surfaces in air were obtained with a Digital Instruments D3000 atomic force microscope (AFM). The root-mean-square (RMS) surfaces roughness values were calculated using Nanoscope Analysis software.

Scanning Electron Microscopy. Surface morphology of CNF and copolymer-CNF were examined using scanning low energy electron microscopy (SLEEM) with a FEI XHR-Verios 460L unit. As the electron beam energy is lowered, the total secondary electron is increased relative to the primary beam. As a result, the interaction volume becomes confined to the nanoscale dimensions. The electron signal originate from a layer very local to the sample, and the image is more representative of the actual surface structure. More specifically, CNF deposited on gold supports were imaged at 100 V. The low electron landing energy excited secondary electrons from the low atomic mass cellulose (relative to the metal support) to produce images with excellent resolution without any metal sputtering on the specimen.

Protein Adsorption. In our previous reports,[32,34] we prepared affinity chromatography systems with HWRGWV as a ligand to purify IgG from IgG-spiked mammalian cell culture medium (cMEM), which contained 10% fetal calf serum and 5% tryptose phosphate broth. We found that BSA was the main contaminant in IgG purification and had a much higher binding affinity with the peptide than any other of the proteins present in cMEM. Therefore, in this work, we chose BSA as a representative nonspecific protein to study the detection of hIgG target molecule. A new buffer (denoted as PBSS) was prepared by adding an additional 1 M NaCl to the phosphate buffer saline (PBS, containing 0.14 M NaCl, Sigma-Aldrich). The presence of excess NaCl in PBSS greatly decreases nonspecific electrostatic binding of BSA.[34] hIgG and BSA were dissolved at different concentrations in PBSS. Protein adsorption on peptide-CNF surfaces was determined using a Q-sense E4 system (Gothenburg, Sweden). The peptide-CNF modified QCM chips were mounted and stable baseline signal was confirmed during the prewashing step with PBSS running buffer at 25 °C. Adsorption experiments with hIgG and BSA were conducted by injecting the respective protein solution in the QCM chamber at a flow rate of 50 μL min^{-1}. At the end of the experiment protein running solution was replaced with the injection of PBSS. Time-resolved changes in the shift of resonant frequency at different overtone number (Δf_n) were recorded and analyzed using the "solidified liquid layer" model to quantify the surface excess, as proposed recently by Ma et al.[36]

RESULTS AND DISCUSSION

Preparation and Characterization of Peptide-CNF Surfaces. Previous studies indicated that CNF exhibits good biocompatibility and low nonspecific protein resistance;[13] these facts suggest the potential use of CNF as substrate in bioactive

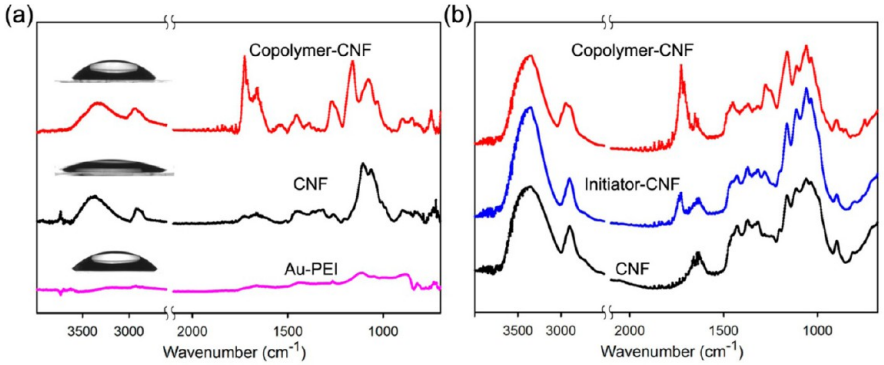

Figure 1. (a) ATR-FTIR spectra of samples obtained from the different modification steps in Method I. Water contact angle images of the respective system are shown as insets. (b) FTIR spectra of CNF after the different modification steps in Method II..

films or nanopaper.[12] In our work, we choose the short peptide, Ac-HWRGWVA, as a ligand for hIgG detection. This peptide has been identified to exhibit high selectively and affinity to the Fc region of hIgG.[33] The peptide was immobilized on CNF using a random copolymer of poly(AMA-*co*-HEMA) as spacer. The two methods used for grafting are illustrated in Scheme 1.

In Method I, the unmodified CNF was spin-coated on PEI-modified QCM chips, followed by attachment of the BIBB initiator to CNF in the presence of TEA and DMAP. This achieved initiator-CNF surface, which was then grafted with poly(AMA-*co*-HEMA) spacer via ARGET-ATRP. Finally, the peptide was immobilized to AMA segments via covalent amide bonds using HATU chemistry.[27,28,37] In Method II, CNF was modified with the copolymer and peptide in aqueous suspension first and then the resultant peptide-CNF was spin-coated on the QCM chip. The surfaces prepared following these two methods are abbreviated as peptide-CNF (I) and peptide-CNF (II), and their surface properties and hIgG binding capability are characterized and compared.

The success of CNF modification by the two different methods was confirmed by ATR-FTIR (or FTIR) and WCA. As shown in Figure 1a, compared with PEI-modified QCM surface (Au-PEI), the appearance of characteristic bands at 3367 cm^{-1} (ν_{O-H}), 2904 cm^{-1} (ν_{C-H}), and the peak at 1062 cm^{-1} (ν_{C-O}) indicated that CNF was successfully coated on the metal. After polymerization, the strong signal peak at 1725 cm^{-1} ($\nu_{C=O}$) confirmed that the random copolymer was grafted from the CNF surfaces. The change in surface wettability further validated the modification process: after CNF deposition on the Au-PEI support, the WCA decreased from 48 ± 2° to 25 ± 3°; the hydrophilicity of CNF is in agreement with previous reports.[21] After copolymer grafting, the WCA increased to 45 ± 7°, which is quite similar to the value measured when the same copolymer was grafted directly from gold surfaces (48 ± 2°).[28] The FITR spectra obtained after the different modification steps used in Method II are shown in Figure 1b. Compared with unmodified CNF, the appearance of a peak at 1725 cm^{-1} ($\nu_{C=O}$) in the spectrum of the initiator-CNF indicates the formation of ester bonds between BIBB and OH groups of CNF, suggesting the covalent binding of the initiator to CNF. Furthermore, the increased intensity of this peak in the spectrum of copolymer-CNF suggests successful copolymer grafting.

The surface morphology and roughness (expressed as the root mean squared (RMS) roughness from AFM imaging) of CNF and modified CNF were analyzed via AFM and SLEEM. It was found that the CNF surface exhibited a typical fibrillar network nanostructure with a RMS roughness of 3.23 ± 0.4 nm (Figure 2a,a′). The nanofibrils were randomly oriented with an average diameter of 33 ± 5 nm (several tens of individual nanofibrils were identified and section analyses were applied to

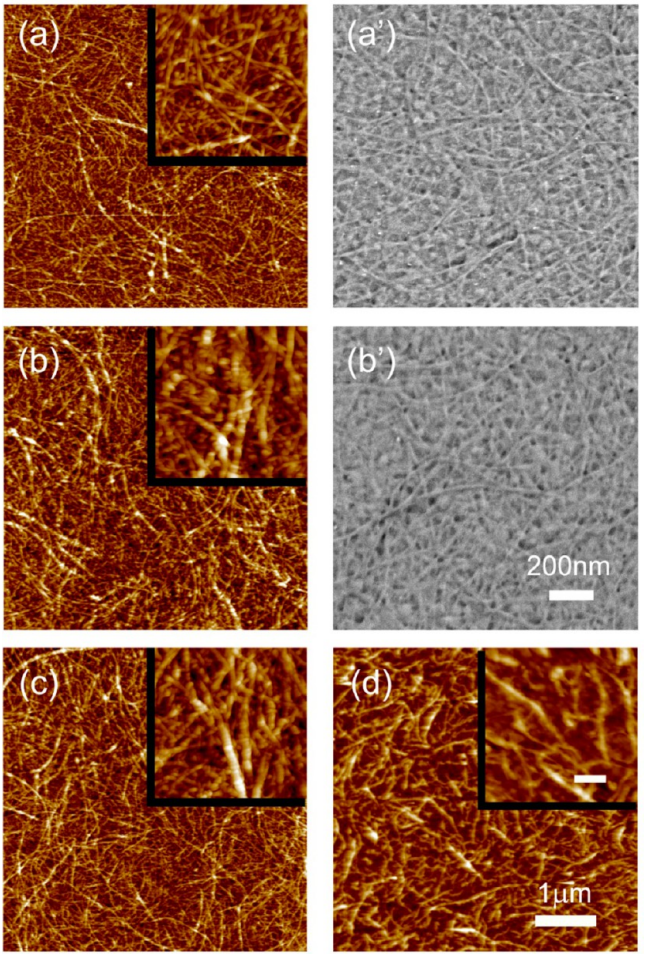

Figure 2. Surface morphology of unmodified (pristine) and modified CNF surfaces. (a–d) AFM height images of (a) CNF, (b) copolymer-CNF, (c) peptide-CNF (I), and (d) peptide-CNF (II) surfaces. The insets in the AFM images correspond to enlarged views with a scale bar of 200 nm. The vertical Z contrast (dark to light) range for all images is −15 to 15 nm. (a′) and (b′) SLEEM images of CNF and copolymer-CNF on gold supports (note the underlying grainy gold metal), respectively.

dx.doi.org/10.1021/bm4007979 | *Biomacromolecules* XXXX, XXX, XXX–XXX

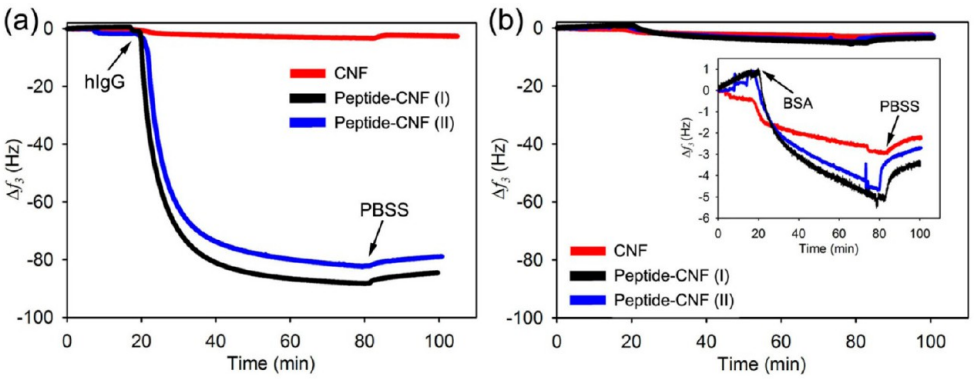

Figure 3. Time-resolved QCM isotherms for adsorption and binding of (a) hIgG and (b) BSA on CNF, peptide-CNF (I), and peptide-CNF (II) surfaces. The inset image in (b) corresponds to an enlarged view of BSA adsorption experiments. Injection of hIgG or BSA solutions as well as rinsing with PBSS buffer is indicated with arrows at the given times.

determine the average diameter and standard deviation). The surface was scanned at several different locations and the profiles were similar at all locations on the film, indicating a homogeneous structure. After polymerization, the nanofibers showed a ring-like structure (inset Figure 2b) and an increased AFM average diameter of 54 ± 14 nm. From SLEEM images it was observed that the copolymer-CNF surface preserved the nanofibrillar structure, although it was fuzzier compared to that of the CNF (Figure 2b′), which is explained by the fact that the grafted polymers "smooth out" the surface, resulting in reduced surface roughness and contrast.[38] The conjugation of the peptide produced a further increase of diameter of the fiber, to 67 ± 12 nm, but did not result in obvious differences in fibril morphology (Figure 2c). The peptide-CNF (II) images obtained from Method II (Figure 2d and Figure S1 in Supporting Information) indicated a less dense network compared with that of peptide-CNF (I).

Protein Adsorption on Peptide-CNF Surface. Our previous studies have demonstrated that peptide-based gold surfaces are capable to detect hIgG from buffer solutions at concentrations lower than 0.05 mg/mL while maintaining nonspecific protein resistance.[28] The use of CNF as supporting material for immobilization of bioactive molecules is however of greater interest given its good biocompatibility, high surface area, and possibility to develop (flexible) bioactive nanopapers or paper-based sensors.[39] The binding capability of target molecule hIgG and the adsorption of nonspecific protein BSA on peptide-CNF were examined by using the QCM technique. The adsorption of protein on the surface leads to a decrease in the QCM resonator frequency, which can be monitored in situ and in real time.[40] In this study, all QCM measurements were conducted at the third overtone and the frequency changes reported as Δf_3. The binding levels of hIgG and BSA on peptide-CNF films prepared according to Methods I and II as well as on films of unmodified CNF (used as reference) are compared in Figure 3.

As shown in Figure 3, the adsorption of hIgG and BSA on reference CNF surfaces only induced 2 Hz change in $-\Delta f_3$, indicating that CNF has good nonspecific protein resistance. This is a remarkable results since it is comparable to well-studied nonfouling polymers such as poly(2-hydroxyethyl methacrylate) (poly(HEMA)) and poly(oligo(ethylene glycol) methacrylate) (poly(OEGMA)) (Figure S2 in Supporting Information). This excellent antifouling property of CNF is suggested to be the result from the abundance of OH groups, providing a hydration layer that prevents access of proteins to the surface. After peptide immobilization, a significant change was observed upon the introduction of hIgG: a shift in frequency ($-\Delta f_3$) of up to 85 and 78 Hz for peptide-CNF (I) and peptide-CNF (II), respectively was recorded (Figure 3a). In contrast, BSA adsorption on the peptide-CNF surface is limited ($-\Delta f_3$ is ∼3 Hz), similar to that on unmodified CNF surface ($-\Delta f_3$ is ∼2 Hz).

Here we used "solidified liquid layer" model[36] to calculate the wet mass of protein (protein with coupled water) adsorbed since this model can decouple the effect of viscoelasticity and allow quantification of the actual changes in wet mass from QCM data upon molecular adsorption on the surfaces from the solution medium (the detailed calculation can be found as Supporting Information). The binding capacity for hIgG (and any coupled water) by the peptide-CNF surfaces was determined to be about 15.1 mg/m^2 (Figure S4 and Scheme S1 in Supporting Information). In contrast, limited adsorption of BSA (less than 0.6 mg/m^2) was detected on both peptide-CNF surfaces (Figure 3b). These results demonstrate that the peptide-CNF exhibits high specific binding ability with hIgG. This is attributed to the specificity of the short peptide and the low noise from nonspecific interactions due to the antifouling background provided by both CNF and the copolymer spacer (Figure S3 in Supporting Information). In addition, it was found that peptide-CNF obtained by Methods I and II have similar hIgG binding levels. Since it is much easier to clean copolymer-CNF surfaces than to purify functionalized CNF in suspension (less solvent and time are required), we selected Method I to prepare the peptide-CNF used in the investigations to be discussed in the next sections. Nevertheless, it is worth noting that that conjugation of peptide to CNF obtained in Method II can be performed in aqueous medium, making the reaction easily scalable and facilitating the manufacture of such bioactive films or nanopaper.

Effect of Initiator Concentration and Copolymer Thickness. Previous research indicated that graft density and thickness of end-grafted polymer brushes were two important factors determining surface properties such as wettability, adhesion, and the final performance of sensor matrices.[41−44] Therefore, in this study, we prepared a series of samples with varying initiator concentration (which is related to the graft density) and thicknesses to systematically investigate their influence on the performance of peptide-CNF for specific

dx.doi.org/10.1021/bm4007979 | Biomacromolecules XXXX, XXX, XXX−XXX

binding of hIgG using BSA as a reference for nonspecific protein adsorption.

The surface density of initiator, which further determine the graft density of copolymer chains, was adjusted by the volume of precursor with initiator group (BIBB) used in the reaction.[45] In this way, a series of copolymer-CNF with different graft densities were prepared, followed by conjugation of peptide, as described before. Figure 4 includes results of binding of hIgG and BSA as a function of BIBB volume. An increased volume of BIBB initiator (corresponding to an increasing graft density) did not lead to a significant change in hIgG adsorption; however, a gradual decrease in BSA adsorption was observed, suggesting an enhanced nonspecific protein resistance. It should be noted that a high volume of BIBB (60 μL) for reaction may compromise the gold layer on the chip, due to erosion (note: in this case, the use of new QCM chips is recommended). The remaining of the discussion considers the case of 40 μL of BIBB, which was employed for further sample preparation.

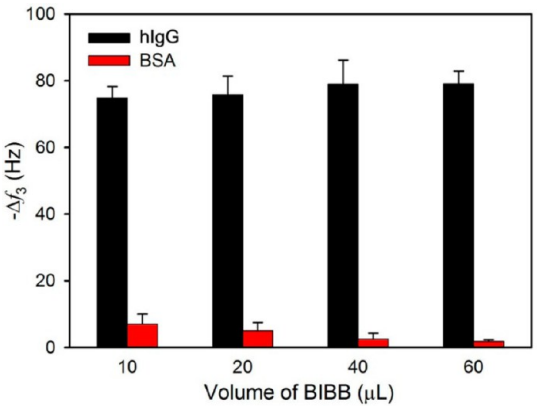

Figure 4. Effect on hIgG and BSA binding of BIBB initiator volume used in the synthesis of peptide-CNF.

Besides initiator concentration, the thickness of the grafted polymer layer is a critical factor in the resultant bioactivity of the system. A series of surfaces were prepared by using different polymerization times. The thicknesses of the copolymer layers ($T_{polymer}$) were determined by ellipsometry and plotted as a function of the polymerization time (Figure 5a). An approximately linear increase in thickness of the grafted layer thickness was observed with increasing polymerization time, up to 60 min; this suggests that the ARGET-ATRP grafting of HEMA and AMA from the initiator-CNF surface was a "controlled" process. The polymerization rate decreased after long polymerization times (beyond ca. 60 min), which may be due to the consumption of the active chain ends via bimolecular reactions.[46] The effect of $T_{polymer}$ on protein adsorption is shown in Figure 5b. There is no significant difference in hIgG adsorption with varying $T_{polymer}$, except for the sample with the thinnest grafted layer (~2.6 nm). For this sample, the grafted copolymer chains are too short to cover CNF, with its low protein affinity, resulting in the lowest IgG adsorption. In contrast, BSA adsorption decreased as $T_{polymer}$ increased and reached almost null adsorption levels for the sample with $T_{polymer}$ at 20.1 nm.

Considering the results of protein adsorption, we conclude that the increase in grafting density and thickness of the spacer polymer had a negligible effect on hIgG binding, while a more extensive suppression of BSA adsorption took place. These observation might be attributed to the difference in the size of the proteins (14.5 × 8.5 × 4 nm^3 for hIgG (MW = ~160 kDa),[47] compared to 14 × 4 × 4 nm^3 for BSA (MW = ~66 kDa)[48]) according to Halperin's model.[49] It is proposed that there are three generic models for protein adsorption: primary adsorption occurring close to the substrate surface, secondary adsorption taking place at the top layer of the polymer brushes, and tertiary adsorption, in which proteins diffuse into the brushes and attach to the grafted chains. For relatively small proteins (in our case, BSA), primary and tertiary adsorption would be of particular importance, which may be reduced by increasing the grafting density, consistent with the model's prediction and previous experimental results. For larger proteins (in our case, hIgG), secondary adsorption is dominant and most of the macromolecules are adsorbed on the outermost surface of the polymer layer. Furthermore, the adsorbed hIgG on the topmost layer would block further access to incoming hIgG molecules to the interior of the polymer matrix due to steric hindrance. The observed limited effect of graft density and thickness of copolymer-CNF on hIgG adsorption is similar to our previous report.[27]

hIgG Binding Affinity with Peptide-CNF. The affinity constant (K_A) between modified CNF and target molecules is an important factor to determine the performance in nanopaper and biosensors. K_A should be high enough to ensure the specific binding of target molecules, but not too high to avoid problems in the separation of target molecules during regeneration and

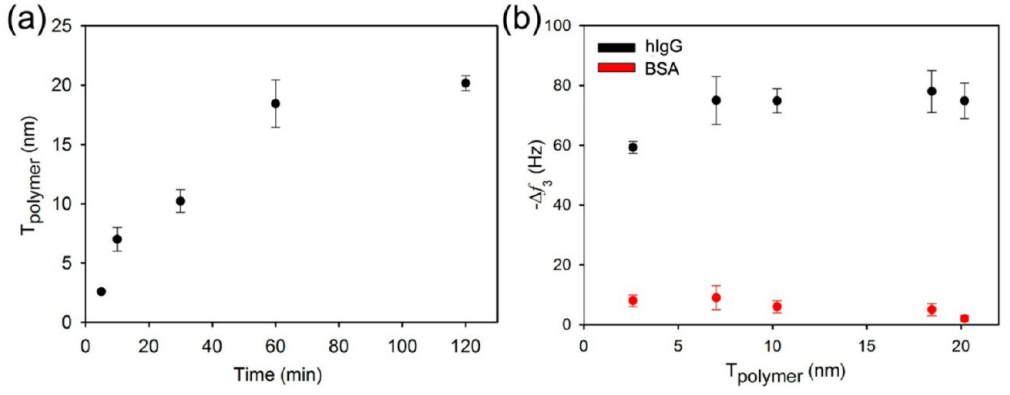

Figure 5. Effect of the thickness of the grafted copolymer ($T_{polymer}$) on protein adsorption. (a) The dependence of $T_{polymer}$ on polymerization time; (b) adsorption of hIgG and BSA on peptide-CNF surfaces with different $T_{polymer}$.

dx.doi.org/10.1021/bm4007979 | Biomacromolecules XXXX, XXX, XXX–XXX

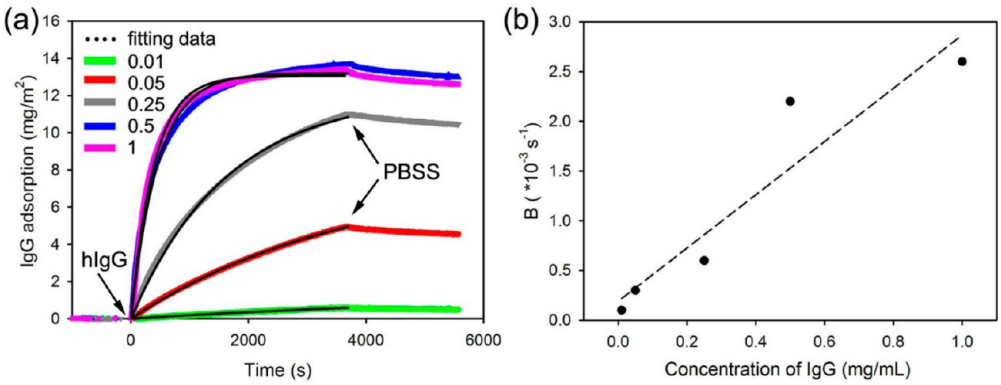

Figure 6. Adsorption isotherms and respective model fits for affinity and kinetic rate constants in QCM experiments. (a) The binding curves were reconstructed from QCM and fitted according to eq 1 (black lines). (b) The fitted values from (a) were adjusted to eq 2, resulting in $k_a = 4.5 \times 10^{-3}$ mg^{-1} mL s^{-1}, $k_d = 1.23 \times 10^{-4}$ s^{-1}, and $K_A = 5.4 \times 10^5$ M^{-1}.

for multiple uses or purification of target molecules. In this study, the effect of hIgG concentration on peptide-facilitated binding was examined by QCM using hIgG solutions of varying concentrations (ranging from 0.01 to 1 mg/mL). $-\Delta f_3$ reached a maximum of 73 Hz for [hIgG] = 0.5 mg/mL, while for a control experiment with BSA (0.5 mg/mL), $-\Delta f_3$ was only 2 Hz, suggesting that the peptide-CNF surface binds hIgG specifically while resisting the nonspecific protein adsorption. QCM signals were found to be sensitive to hIgG binding: noticeable frequency shifts, equivalent to −26 and −3 Hz, were recorded for [hIgG] at 0.05 and 0.01 mg/mL.

The affinity and kinetic rate constants were calculated based on the QCM results and fitted to eqs 1 and 2:[41,50]

$$\Delta M = \frac{k_a C \Delta M_{max}}{(k_a C + k_d)}(1 - \exp[-(k_a C + k_d)t]) \quad (1)$$

$$B = k_a C + k_d \quad (2)$$

where C is the concentration of hIgG; $-\Delta M_{max}$ and $-\Delta M$ corresponds to the maximum and measured binding amount of hIgG, respectively; k_a and k_d are the binding kinetics constant and the disassociation constant, respectively; and t is the measuring time.

All the QCM experimental curves were well fitted ($R^2 > 0.98$) according to eq 1, and the fitted values were further linearly fitted according to eq 2 ($R^2 = 0.94$), as shown in Figure 6. The calculated k_a and k_d were 4.5×10^{-3} mg^{-1} mL s^{-1} and 1.23×10^{-4} s^{-1}, respectively. The calculated affinity constant ($K_A = k_a/k_d$) between hIgG and peptide-CNF was 5.4×10^5 M^{-1}, which is similar with that obtained for similar short peptide systems supported on metals (4.9×10^5 M^{-1}).[28] However, differences in the values of k_a and k_d for the CNF-based and metal-based systems are noted. It can be speculated that this observation may be due to differences in the substrate type (fibril network structure in CNF compared to the smooth metal substrates) but the detailed mechanism of binding is outside the scope of this contribution. More importantly, the obtained K_A is lower than that between protein A and hIgG ($\sim 10^7$–10^8 M^{-1}), suggesting that recovery of hIgG from the CNF surface can be carried out under milder elution conditions in which the loss of activity and protein aggregation (typically observed in low pH elution buffers) can be depressed.[32,34] These results may be taken as ideal for the purification of hIgG when using peptide-CNF as static phase in chromatography.

CONCLUSIONS

The modification of CNF with poly(AMA-*co*-HEMA) and its potential use as substrate for bioactive films or nanopaper were investigated after conjugating short peptide ligands with specific affinity with hIgG. The peptide was conjugated to CNF via poly(AMA-*co*-HEMA) as spacer by two methods. The adsorption of protein on the resultant peptide-CNF was examined using QCM, and the results indicated that these surfaces have specific hIgG binding capability while maintaining very good nonspecific protein resistance. To optimize the hIgG binding ability while minimizing the nonspecific BSA adsorption, the graft density and thickness of the copolymer spacer on CNF were adjusted. The results indicated that the density and thickness of the spacer polymer slightly affected the binding capability of hIgG; therefore, hIgG is expected to bind to peptide-CNF on the topmost layer. In contrast, BSA shows negligible adsorption on peptide-CNF prepared with a high grafting density and thickness of poly(AMA-*co*-HEMA). Moreover, the developed peptide-CNF can detect hIgG in PBSS buffer at concentrations lower than 0.05 mg/mL. The affinity constant of peptide-CNF for hIgG is 5.4×10^5 M^{-1}, suggesting that copolymer-modified CNF has no influence on the binding affinity between hIgG and the peptide ligand. Overall, the proposed bioactive peptide-CNF is expected to offer a new platform for low cost and disposable CNF-based sensor or nanopaper for detection of hIgG and also for the development of other inexpensive and sustainable bioactive materials. Considering the unique properties of CNF, our continuing research is directed toward extending this methodology to various applications such as using CNF as static phase in chromatography.

ASSOCIATED CONTENT

Supporting Information

AFM images of peptide-CNF (method II) spin coated onto the substrate. The adsorption isotherms for BSA on poly(OEGMA), poly(HEMA), and pristine CNF surfaces are introduced. A comparison of protein adsorption on peptide-CNF surfaces with poly(AMA) and poly(AMA-*co*-HEMA) as spacer and calculation of protein adsorption with "solidified liquid layer" model are also included. This material is available free of charge via the Internet at http://pubs.acs.org.

dx.doi.org/10.1021/bm4007979 | *Biomacromolecules* XXXX, XXX, XXX–XXX

AUTHOR INFORMATION

Corresponding Author

*E-mail: ojrojas@ncsu.edu (O.J.R.); yzhang58@ncsu.edu (Y.Z.). Tel.: +1-919-5137494. Fax: +1- 919-515 6302.

Notes

The authors declare no competing financial interest.

ACKNOWLEDGMENTS

This research was supported by North Carolina Biotechnology Center, Grant 2012-0049/2012-MRG-1105. We thank Profs. J. Genzer and K. Efimenko (NCSU) for access to ellipsometer facilities and Prof. Jon-Paul Maria (NCSU) for the SLEEM measurement. Y.Z. also thanks Dr. Q. Yu for helpful discussion and input.

REFERENCES

(1) Turbak, A. F.; Snyder, F. W.; Sandberg, K. R. *J. Appl. Polym. Sci.: Appl. Polym. Symp.* **1983**, *37*, 815−827.
(2) Saito, T.; Kimura, S.; Nishiyama, Y.; Isogai, A. *Biomacromolecules* **2007**, *8*, 2485−2491.
(3) Klemm, D.; Kramer, F.; Moritz, S.; Lindström, T.; Ankerfors, M.; Gray, D.; Dorris, A. *Angew. Chem., Int. Ed.* **2011**, *50*, 5438−5466.
(4) Lavoine, N.; Desloges, I.; Dufresne, A.; Bras, J. *Carbohydr. Polym.* **2012**, *90*, 735−764.
(5) Klemm, D.; Heublein, B.; Fink, H.-P.; Bohn, A. *Angew. Chem., Int. Ed.* **2005**, *44*, 3358−3393.
(6) Roy, D.; Semsarilar, M.; Guthrie, J. T.; Perrier, S. *Chem. Soc. Rev.* **2009**, *38*, 2046−2064.
(7) Yano, H.; Nakahara, S. *J. Mater. Sci.* **2004**, *39*, 1635−1638.
(8) Syverud, K.; Stenius, P. *Cellulose* **2009**, *16*, 75−85.
(9) Stenstad, P.; Andresen, M.; Tanem, B. S.; Stenius, P. *Cellulose* **2008**, *15*, 35−45.
(10) Pahimanolis, N.; Hippi, U.; Johansson, L. S.; Saarinen, T.; Houbenov, N.; Ruokolainen, J.; Seppälä, J. *Cellulose* **2011**, *18*, 1201−1212.
(11) Orelma, H.; Filpponen, I.; Johansson, L.; Österberg, M.; Rojas, O.; Laine, J. *Biointerphases* **2012**, *7*, 61.
(12) Orelma, H.; Johansson, L. S.; Filpponen, I.; Rojas, O. J.; Laine, J. *Biomacromolecules* **2012**, *13*, 2802−2810.
(13) Arola, S.; Tammelin, T.; Setälä, H.; Tullila, A.; Linder, M. B. *Biomacromolecules* **2012**, *13*, 594−603.
(14) Valo, H.; Kovalainen, M.; Laaksonen, P.; Häkkinen, M.; Auriola, S.; Peltonen, L.; Linder, M.; Järvinen, K.; Hirvonen, J.; Laaksonen, T. *J. Controlled Release* **2011**, *156*, 390−397.
(15) Kolakovic, R.; Peltonen, L.; Laaksonen, T.; Putkisto, K.; Laukkanen, A.; Hirvonen, J. *AAPS Pharm.* **2011**, *12*, 1366−1373.
(16) Bhattacharya, M.; Malinen, M. M.; Lauren, P.; Lou, Y. R.; Kuisma, S. W.; Kanninen, L.; Lille, M.; Corlu, A.; GuGuen-Guillouzo, C.; Ikkala, O.; Laukkanen, A.; Urtti, A.; Yliperttula, M. *J. Controlled Release* **2012**, *164*, 291−298.
(17) Diez, I.; Eronen, P.; Österberg, M.; Linder, M. B.; Ikkala, O.; Ras, R. H. A. *Macromol. Biosci.* **2011**, *11*, 1185−1191.
(18) Ahola, S.; Salmi, J.; Johansson, L. S.; Laine, J.; Österberg, M. *Biomacromolecules* **2008**, *9*, 1273−1282.
(19) Aulin, C.; Ahola, S.; Josefsson, P.; Nishino, T.; Hirose, Y.; Österberg, M.; Wågberg, L. *Langmuir* **2009**, *25*, 7675−7685.
(20) Ahola, S.; Myllytie, P.; Österberg, M.; Teerinen, T.; Laine, J. *Bioresources* **2008**, *3*, 1315−1328.
(21) Johansson, L. S.; Tammelin, T.; Campbell, J. M.; Setälä, H.; Österberg, M. *Soft Matter* **2011**, *7*, 10917−10924.
(22) Beeck, H.; Hellstern, P. *Vox Sang.* **1998**, *74*, 219−223.
(23) Burton, D. R. *Mol. Immunol.* **1985**, *22*, 161−206.
(24) Shiang, Y. C.; Lin, C. A.; Huang, C. C.; Chang, H. T. *Analyst* **2011**, *136*, 1177−1182.
(25) Bayry, J.; Thirion, M.; Misra, N.; Thorenoor, N.; Delignat, S.; Lacroix-Desmazes, S.; Bellon, B.; Kaveri, S.; Kazatchkine, M. D. *Neurol. Sci.* **2003**, *24*, s217−s221.
(26) Haab, B. B. *Proteomics* **2003**, *3*, 2116−2122.
(27) Zhang, Y.; Islam, N.; Carbonell, R. G.; Rojas, O. J. *ACS Appl. Mater. Interfaces* **2013**, *5*, 8030−8037.
(28) Zhang, Y.; Islam, N.; Carbonell, R. G.; Rojas, O. J. *Anal. Chem.* **2013**, *85*, 1106−1113.
(29) Carlmark, A.; Malmström, E. *J. Am. Chem. Soc.* **2002**, *124*, 900−901.
(30) Carlmark, A.; Malmström, E. E. *Biomacromolecules* **2003**, *4*, 1740−1745.
(31) Yang, H.; Gurgel, P. V.; Carbonell, R. G. *J. Pept. Res.* **2005**, *66*, 120−137.
(32) Yang, H. O.; Gurgel, P. V.; Carbonell, R. G. *J. Chromatogr., A* **2009**, *1216*, 910−918.
(33) Yang, H. O.; Gurgel, P. V.; Williams, D. K.; Bobay, B. G.; Cavanagh, J.; Muddiman, D. C.; Carbonell, R. G. *J. Mol. Recognit.* **2010**, *23*, 271−282.
(34) Naik, A. D.; Menegatti, S.; Gurgel, P. V.; Carbonell, R. G. *J. Chromatogr., A* **2011**, *1218*, 1691−1700.
(35) Liu, Z.; Gurgel, P. V.; Carbonell, R. G. *J. Chromatogr., A* **2011**, *1218*, 8344−8352.
(36) Ma, H. W.; He, J. A.; Zhu, Z. Q.; Lv, B. E.; Li, D.; Fan, C. H.; Fang, J. *Chem. Commun.* **2010**, *46*, 949−951.
(37) Valeur, E.; Bradley, M. *Chem. Soc. Rev.* **2009**, *38*, 606−631.
(38) Hansson, S.; Ostmark, E.; Carlmark, A.; Malmström, E. *ACS Appl. Mater. Interfaces* **2009**, *1*, 2651−2659.
(39) Pelton, R. *TrAC, Trends Anal. Chem.* **2009**, *28*, 925−942.
(40) Ward, M. D.; Buttry, D. A. *Science* **1990**, *249*, 1000−1007.
(41) Ma, H.; He, J. A.; Liu, X.; Gan, J.; Jin, G.; Zhou, J. *ACS Appl. Mater. Interfaces* **2010**, *2*, 3223−3230.
(42) Coad, B. R.; Lu, Y.; Glattauer, V.; Meagher, L. *ACS Appl. Mater. Interfaces* **2012**, *4*, 2811−2823.
(43) Yu, Q.; Zhang, Y. X.; Chen, H.; Wu, Z. Q.; Huang, H.; Cheng, C. *Colloids Surf., B* **2010**, *76*, 468−474.
(44) Huang, C. J.; Li, Y. T.; Jiang, S. Y. *Anal. Chem.* **2012**, *84*, 3440−3445.
(45) Zoppe, J. O.; Österberg, M.; Venditti, R. A.; Laine, J.; Rojas, O. J. *Biomacromolecules* **2011**, *12*, 2788−2796.
(46) Xu, F. J.; Zhong, S. P.; Yung, L. Y. L.; Kang, E. T.; Neoh, K. G. *Biomacromolecules* **2004**, *5*, 2392−2403.
(47) Lee, K. B.; Park, S. J.; Mirkin, C. A.; Smith, J. C.; Mrksich, M. *Science* **2002**, *295*, 1702−1705.
(48) Huang, M.; He, J. A.; Gan, J. H.; Ma, H. W. *Colloids Surf., B* **2011**, *85*, 92−96.
(49) Halperin, A. *Langmuir* **1999**, *15*, 2525−2533.
(50) Shen, Z.; Mernaugh, R. L.; Yan, H.; Yu, L.; Zhang, Y.; Zeng, X. *Anal. Chem.* **2005**, *77*, 6834−6842.